Nonlinear Effects in Interference of Bose-Einstein Condensates

Wu-Ming Liu,[1,2] Biao Wu,[1] and Qian Niu[1]

[1]*Department of Physics, The University of Texas at Austin, Austin, Texas 78712-1081*
[2]*Institute of Theoretical Physics, Chinese Academy of Sciences, P.O. Box 2735, Beijing 100080, China*
(Received 27 October 1999)

Nonlinear effects in the interference of Bose-Einstein condensates are studied using exact solutions of the one-dimensional nonlinear Schrödinger equation, which is applicable when the lateral motion is confined or negligible. With the inverse scattering method, the interference pattern is studied as a scattering problem with the linear Schrödinger equation, whose potential is profiled by the initial density distribution of the condensates. Our theory not only provides an analytical framework for quantitative predictions for the one-dimensional case, it also gives an intuitive understanding of some mysterious features of the interference patterns observed in experiments and numerical simulations.

The nonlinear Schrödinger equation has been a paradigm of theoretical and experimental studies of coherent nonlinear dynamics [1]. The realization and rapid development of Bose-Einstein condensates (BEC) of alkaline atoms have provided a new stage for practical applications of this equation [2]. Almost all of these theoretical studies have been based on numerical solutions, which are necessary for two- and three-dimensional problems and for cases with external driving forces. On the other hand, there has been tremendous progress in the past thirty years in developing analytical methods, such as the inverse scattering method, for finding exact solutions of one-dimensional nonlinear systems [3,4]. It remains to be seen how these analytical results can impact on our understanding of coherent dynamics of the alkaline BEC packets.

In this Letter, we apply the inverse scattering method to the problem of interference of BEC wave packets. The interference of three-dimensional BEC packets was observed recently [5]; the one-dimensional situation can be achieved experimentally either by maintaining the lateral confinement of cigar-shaped BEC packets during the interference process or by using condensates whose lateral dimensions are large compared with the gap between them such that there is little lateral expansion before the two BEC packets merge together. Our theory not only yields analytical predictions on how interatomic interactions affect the interference fringes for one-dimensional experiments in the future, it also provides an intuitive understanding of some mysterious features of the interference patterns observed in experiment [5] and in numerical simulations [6,7].

The basic idea of the inverse scattering method [3,4] is to transform a nonlinear problem into a linear scattering problem. In our case, the one-dimensional nonlinear Schrödinger equation is transformed into a linear Schrödinger scattering problem whose potential is of double-barrier shape profiled by the initial density distribution of BEC packets. We argue that the interference of BEC packets is a long-time behavior and, therefore, is described by the asymptotic solution of the nonlinear Schrödinger equation. This asymptotic solution has an exact form in

terms of the reflection coefficient of the linear scattering problem [8], so we are able to study the interference pattern by calculating the reflection coefficient for the double-barrier potential.

Theoretical formulation.—Our starting point is the nonlinear Schrödinger equation or the Gross-Pitaevskii equation [9], whose numerical simulation has previously produced good agreement with experimental interference data [7]. For theoretical exploration beyond the mean field level, the reader is referred to Refs. [10,11]. In scaled form, the one-dimensional motion of the condensate wave function ϕ is governed by

$$i\frac{\partial\phi}{\partial t} = -\frac{1}{2}\frac{\partial^2\phi}{\partial x^2} + g|\phi|^2\phi, \qquad (1)$$

where x is measured in units of $\xi = 1\ \mu$m, a characteristic length unit in this type of experiment, t in units of $\frac{m\xi^2}{\hbar}$ (m is the atomic mass), ϕ in units of the square root of $n_0 aaa$, the maximum density in the initial distribution of the condensate, and the interaction constant is defined as $g = 4\pi n_0 a\xi^2$, with $a > 0$ being the interatomic scattering length. With this choice of units, the unit for momentum is $\hbar/m\xi$; the constant $g = 5-10$ and the time of flight $t \approx 120$ in the experiment of Ref. [5].

In Figs. 1(a)–1(c), we plot the results showing how two Gaussian wave packets with zero relative phase evolve according to Eq. (1). The interference pattern forms as early as $t = 9$. After that, $|\phi(x,t)|^2$ merely expands uniformly in space and linearly with time, with its basic profile, the valleys and peaks, remaining unchanged. Note that we made the choice of $g = 2$ in Fig. 1, instead of the larger experimental values, in order to have fewer peaks so that the structure of the curves can be seen more clearly. With higher g, the wave packets expand faster and the interference pattern settles earlier. So, the time of flight $t \approx 120$ in the experiment of Ref. [5] is really a long time as far as the settlement of the interference pattern is concerned. With the aid of exact solutions for the one-dimensional nonlinear Schrödinger equation, we are now able to study this asymptotic regime of interference analytically.
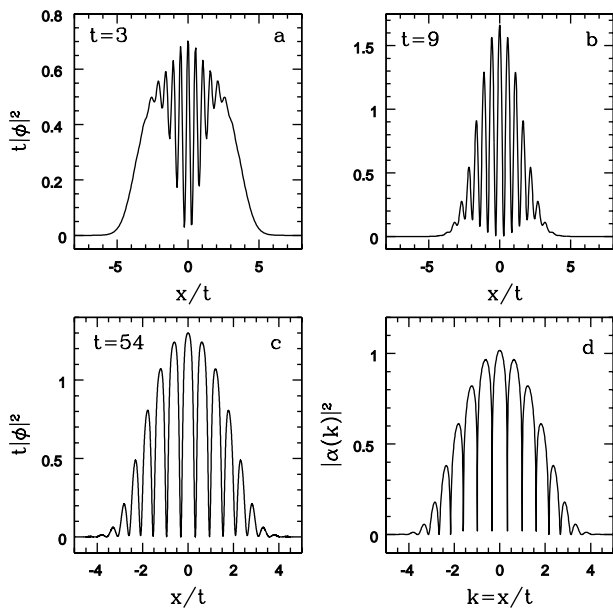

FIG. 1.   Evolution of two BECs ($g = 2, d_0 = 12, \sigma = 1$). The scaled packets at (a) $t = 3$, (b) $t = 9$, and (c) $t = 54$. (d) $|\alpha(k)|^2$ in Eq. (4).

The exact solution for the nonlinear Schrödinger equation (1) can be achieved by the inverse scattering method [8]. Its central step is to solve an auxiliary linear scattering problem defined by the following differential equations:

$$i \frac{\partial \psi_1}{\partial x} + \sqrt{g} \, \phi \psi_2 = \frac{k}{2} \psi_1 \,,$$
$$i \frac{\partial \psi_2}{\partial x} - \sqrt{g} \, \phi^* \psi_1 = -\frac{k}{2} \psi_2 \,, \tag{2}$$

with the boundary conditions: $\psi_1 \rightarrow e^{ikx/2}$ as $x \rightarrow -\infty$ and $\psi_2 \rightarrow 0$ as $x \rightarrow +\infty$. Note that the wave function $\phi(x, t)$ in the nonlinear problem appears as a scattering potential in the linear problem. The reflection and transmission coefficients, $r(k)$ and $\tau(k)$, are defined as the amplitudes in the asymptotic behaviors: $\psi_1 \rightarrow \tau(k)e^{ikx/2}$ as $x \rightarrow +\infty$ and $\psi_2 \rightarrow r(k)e^{-ikx/2}$ as $x \rightarrow -\infty$. This linear scattering problem is designed in such a way that, with $\phi(x, t)$ evolving with time according to the nonlinear equation (1), the magnitude of the reflection coefficient, $|r(k)|$, is invariant. Our subsequent discussions will only require the knowledge of $|r(k)|$, so we can use the initial wave function $\phi(x, 0)$, for the scattering potential.

The long-time asymptotic solution of the nonlinear problem has an exact form as

$$\phi(x, t) = \frac{\alpha(\frac{x}{t})}{\sqrt{t}} e^{i(x^2/2t) - i2|\alpha(x/t)|^2 \log(4t)} + O(t^{-1} \log t) \,, \tag{3}$$

where $\alpha(k = \frac{x}{t})$ is determined by $r(k)$. Because the interference pattern is described completely by the density

distribution $|\phi(x, t)|^2$, it is sufficient to know the magnitude of $\alpha(k)$, which is given by

$$|\alpha(k)|^2 = -\frac{1}{2\pi g} \log(1 - |r(k)|^2) \,. \tag{4}$$

To demonstrate the validity of the above results, we draw in Fig. 1(d), $|\alpha(k)|^2$ obtained directly from the scattering problem Eq. (2), and find an excellent agreement with the quantity $t|\phi|^2$ shown in Fig. 1(c). This coincidence suggests that $|\alpha(k)|^2$ is the long-time asymptotic momentum distribution. This relation is also confirmed directly by a Fourier transform of the wave function (3) with the stationary phase method appropriate for long times. This result states that, as far as long-time distributions are concerned, the fringe spacing Δx in real space and Δk in momentum space are simply related by (in physical units)

$$\frac{\Delta x}{t} = \frac{\hbar}{m} \Delta k \,. \tag{5}$$

Because of this, we will focus on the interference in momentum space from now on. Very recently, a suggestion [12] was made to observe the interference in momentum space with inelastic photon scattering [13].

While the above formulation can deal with arbitrary initial conditions, we will assume for simplicity that the BEC packets have a zero relative phase for the rest of our discussions. The symmetrical distribution of interference patterns in the experiment of Ref. [1] seems to suggest that this may actually be the case for some reason. In any case, one can certainly assume a zero relative phase by considering wave packets split from the same BEC. We are then able to reformulate the scattering problem into a linear Schrödinger equation, for which we can utilize all our physical intuition and mathematical machinery developed in the learning of basic quantum mechanics. By defining $\psi = \psi_1 - i\psi_2$, we find

$$-\frac{d^2 \psi}{dx^2} + (g\phi_0^2 - \sqrt{g} \, \phi_0')\psi = \frac{k^2}{4} \psi \,. \tag{6}$$

This is a linear Schrödinger equation with the potential profiled by the initial wave function of the nonlinear problem, $V(x) = g\phi_0^2 - \sqrt{g} \, \phi_0'$. The reflection coefficient defined before can thus be calculated as a standard quantum scattering problem in one-dimension.

Applications and predictions.—Two properties of the interference pattern can immediately be stated based on Eq. (4): (i) the interference pattern should be symmetrically distributed; (ii) the envelope of the density distribution should be lower at higher values of k. The first stems from the fact that $|r(-k)| = |r(k)|$ for real potentials; the second is because the transmission is generally easier at higher energies. These two properties are general and do not depend on the initial distribution of the BEC packets.

For weak potentials or large momenta, we can calculate the reflection coefficient with the Born approximation.

The momentum density distribution of the interference pattern is then given by

$$|\alpha(k)|^2 \approx \frac{|r(k)|^2}{2g\pi}$$

$$\approx \frac{1}{2g\pi k^2} \left| \int dx(g\phi_0^2 - \sqrt{g}\,\phi_0')e^{ikx} \right|^2. \quad (7)$$

In the limit of $g \to 0$, we can ignore the first term in the potential, and an integration by parts then yields the free particle result that the momentum distribution is that of the initial state. In particular, if the initial wave function consists of two Gaussian wave packets, with separation d_0 and the same width σ, we find that

$$|\alpha(k)|^2 = 4\sigma^2 \cos^2\left(\frac{kd_0}{2}\right)e^{-k^2\sigma^2}, \quad (8)$$

which describes a uniform interference pattern with period $2\pi/d_0$. It is exactly the free particle result obtained in Refs. [6,7].

The more interesting case is when g is big as in the experiment of Ref. [5]. In this case, for energies $\frac{k^2}{4}$ over the peaks of the potential, one can use the WKB method to calculate the overbarrier reflections, yielding

$$|\alpha(k)|^2 \approx \frac{2}{g\pi} e^{-[\pi(k^2/4-g)\sigma/\sqrt{g}]} \cos^2 \int_{-(d_0/2)}^{d_0/2}$$

$$\times dx\left(\frac{k^2}{4} - V(x)\right)^{1/2}. \quad (9)$$

Based on this expression, it is easy to find out that the fringes ($k \gtrsim 2\sqrt{g}$) are uniform for large separations of the two BEC clouds and nonuniform for small separations. It is also clear from the exponential term, which comes from the reflection over one peak, that the distribution decays very fast when the energy $\frac{k^2}{4}$ is higher than the barriers. Therefore, the dominant part of the interference pattern lies in the range of $k < 2\sqrt{g}$, corresponding to energies below the barriers.

Three different cases are shown in the upper panels of Fig. 2 for the scattering potential $V(x) = g\phi_0^2 - \sqrt{g}\,\phi_0'$. In each case the potential has quasibound levels inside the well. Resonant transmission occurs at these levels, where $r(k)$ vanishes, which in turn leads to nodes in the BEC wave function according to Eq. (4). Therefore, by calculating the energies of these quasibound levels, we can obtain the positions and spacings of the fringes in the interference pattern of the BEC wave packets. Figure 2(a) shows the case of two BEC packets initially not far apart ($d_0 = 3.6\sigma$). The potential well can be approximated by a harmonic potential

$$V(x) \approx V_0 + \tfrac{1}{2}V_0''x^2, \quad (10)$$

where V_0 is the potential minimum between the walls and V_0'' is the curvature of the potential at the minimum. So
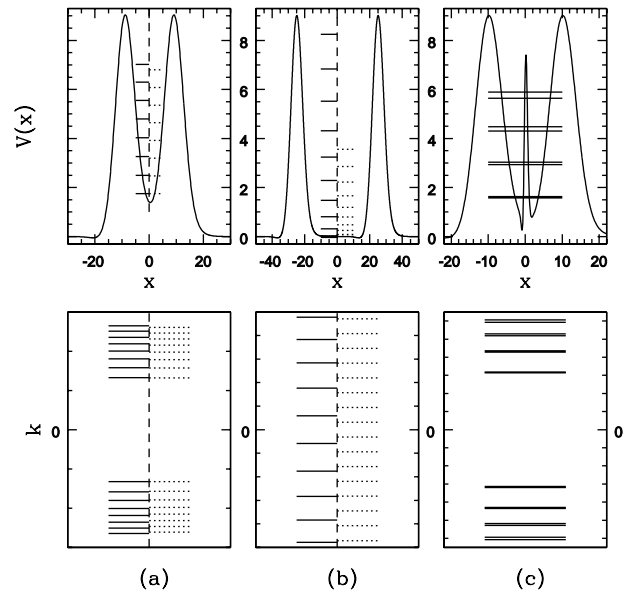

FIG. 2. The potentials, the energy levels, and the levels in k. Two Gaussian wave packets with (a) small separation, (b) large separation, and (c) three Gaussian wave packets. The solid level lines are accurate numerical results while the dotted lines are analytical results for comparison. Note that the energy levels in (b) are magnified by a factor of 10; the k level spacing is the fringe spacing or the interference band in the main text.

the fringe position can be estimated with the energy levels for this harmonic potential,

$$k_{\pm n} = \pm 2\sqrt{E_n} = \pm 2[V_0 + (n - \tfrac{1}{2})\sqrt{2V_0''}]^{1/2}. \quad (11)$$

We plot them in Fig. 2(a) against the accurate levels, and see a very good agreement. Therefore, the central fringe spacing is given by

$$\Delta k_0 = k_1 - k_{-1} = 4(V_0 + \sqrt{V_0''/2})^{1/2}, \quad (12)$$

while the spacings of higher order fringes are given by $\Delta k_n = k_{n+1} - k_n$. The resulting fringe positions are drawn in the lower panel of Fig. 2(a), where we see that the central band is very wide due to the nonzero potential floor V_0, and other bands are much narrower and close to uniformly spaced. We can thus understand why a strong overlap in the initial BEC wave packets can result in the nonuniform patterns as seen in the experiment [5,14] and the numerical simulations [7].

As the initial separation becomes larger, the fringes become more uniformly spaced. The case of $d_0 = 10\sigma$ is shown in Fig. 2(b), where we see that the fringes are almost uniform, but with a spacing much larger than the free particle result, which is drawn with the dotted lines on the right-hand side for comparison. The larger spacing can be understood from the relation $\Delta k = \pi/d^*$, where d^* is the effective width of the well. Near the bottom of the well, where the levels shown in Fig. 2(b) actually lie, the well width is shorter than the distance d between the Gaussian packets by the order of the full width σ of the Gaussians

[6]. This difference eventually becomes negligible for very large separations, yielding level spacings corresponding to the free particle results. These results are also in accordance with our physical intuition: with a large initial separation, the clouds become dilute and less interacting when they meet each other, so the fringes become more like the ones for the noninteracting gas. It is clear now that the uniform pattern shown in the right picture of Fig. 2 in Ref. [5] is due to two factors: the initial large separation and the fast lateral expansion which helps to reduce the density of the condensates.

The width of an interference fringe can be obtained from the linewidth of the corresponding quasibound level, which has a finite lifetime due to tunneling through the potential barriers. Generally speaking, the level width increases with energy, implying thicker fringes on the sides than those near the center. More specifically, the ratio of the level width to the level spacing can be estimated using the WKB method,

$$\frac{\delta k_n}{\Delta k_n} = \frac{\delta E_n}{\Delta E_n} = 2e^{-2\sqrt{g-E_n}w(E_n)}, \tag{13}$$

where $w(E_n)$ is the width of a barrier at the level energy. Because of the exponential dependence, the fringe widths can be extremely narrow for large g and thick wave packets, as is evident from Fig. 1(d). The observation of such narrow widths is a challenge to the experimentalists; the lack of very good optical resolution and system stability will result in the smearing of these narrow valleys in the density distribution and reduced contrast or visibility of the fringes. On the other hand, the development of the narrow valleys seems to require very long times. For the case shown in Fig. 1, one can still see reasonably wide valleys at time $t = 54$ as in Fig. 1(c). There is not a good theory for the time dependence of the widths, although a Heissenberg uncertainty width seems to give the right order of magnitude.

Finally, we would like to mention that we can predict intuitively within this framework the interference patterns for more than two BEC packets. In Fig. 2(c), we plot the case where there are three BEC packets and see the pairing of fringes appearing in the interference. Also. when it is possible to arrange a periodic array of BEC clouds, we may expect to see a "band structure" in the interference pattern.

[1] Special issue, edited by A. V. Mikhailov, E. A. Kuznetsov, A. C. Newell, and V. E. Zakharov, Physica (Amsterdam) **85D**, Nos. 1–4 (1995).

[2] F. Dalfovo, S. Giorgini, L. P. Pitaevskii, and S. Stringari, Rev. Mod. Phys. **71**, 463 (1999).

[3] C. S. Gardner, J. M. Greene, M. D. Kruskal, and R. M. Miura, Phys. Rev. Lett. **19**, 1095 (1967). For detailed accounts of the inverse scattering method, see M. J. Ablowitz and P. A. Clarkson, *Soliton, Nonlinear Evolutions and Inverse Scattering* (Cambridge University Press, Cambridge, England, 1991); A. Das, *Integrable Models* (World Scientific, Singapore 1989).

[4] V. E. Zakharov and A. B. Shabat, Zh. Eksp. Teor. Fiz. **61**, 118 (1971) [Sov. Phys. JETP **34**, 62 (1972)]; V. E. Zakharov and S. V. Manakov, Zh. Eksp. Teor. Fiz. **71**, 203 (1976) [Sov. Phys. JETP **44**, 106 (1976)].

[5] M. R. Andrews, C. G. Townsend, H. J. Miesner, D. S. Durfee, D. M. Kurn, and W. Ketterle, Science **275**, 637 (1997).

[6] H. Wallis, A. Rohrl, M. Naraschewski, and A. Schenzle, Phys. Rev. A **55**, 2109 (1997).

[7] A. Rohrl, M. Naraschewski, A. Schenzle, and H. Wallis, Phys. Rev. Lett. **78**, 4143 (1997).

[8] H. Segur and M. J. Ablowitz, J. Math. Phys. **17**, 714 (1976);*ibid.* 719 (1976); P. A. Deift and X. Zhou, Commun. Math. Phys. **165**, 175 (1995).

[9] E. P. Gross, J. Math. Phys. **4**, 195 (1963); L. P. Pitaevskii, Zh. Eksp. Teor. Fiz. **13**, 451 (1961) [Sov. Phys. JETP **13**, 451 (1961)].

[10] J. Javanainen and S. M. Yoo, Phys. Rev. Lett. **76**, 161 (1996); M. Naraschewski, H. Wallis, A. Schenzle, J. I. Cirac, and P. Zoller, Phys. Rev. A **54**, 2185 (1996); J. I. Cirac, C. W. Gardiner, M. Naraschewski, and P. Zoller, *ibid.* **54**, R3714 (1996); T. Wong, M. J. Collett, and D. F. Walls, *ibid.* R3718 (1996); Y. Castin and J. Dalibard, *ibid.* **55**, 4330 (1997).

[11] M. Lewenstein and L. You, Phys. Rev. Lett. **77**, 3489 (1996); J. Javanainen and M. Wilkens, Phys. Rev. Lett. **78**, 4675 (1997); V. A. Alekseev, Pis'ma Zh. Eksp. Teor. Fiz. **69**, 491 (1999) [JETP Lett. **69**, 526 (1999)].

[12] L. P. Pitaevskii and S. Stringari, Phys. Rev. Lett. **83**, 4237 (1999).

[13] J. Stenger, S. Inouye, A. P. Chikkatur, D. M. Stamper-Kurn, D. E. Pritchard, and W. Ketterle, Phys. Rev. Lett. **82**, 4569 (1999).

[14] Even the mysterious bending feature seen in the left picture of Fig. 2 in Ref. [5] can be explained partially under this picture. With the cigar-shaped BEC packets shown in Fig. 1(A) of Ref. [5], let us consider a slice parallel to the long axis at a distance r. Because the gap between the two BEC packets increases with r, both V_0 and V_0'' diminish as r becomes large. Therefore, the central fringe becomes narrower according to Eqs. (11) and (12), rendering the other fringes bending inward.